NJC

ROYAL SOCIETY OF CHEMISTRY

PAPER

View Article Online
View Journal | View Issue

Cite this: *New J. Chem.*, 2021, 45, 21763

Atomic-scale investigation of the effect of surface carbon coatings on the oxidation and mechanical properties of iron nanowires

Gurcan Aral *[a] and Md Mahbubul Islam [b]

The understanding of the complex atomistic-scale mechanisms of the oxidation process of carbon (C) coated iron nanowires (Fe NW) and also the resulting modulation of mechanical properties is a highly challenging task. We perform reactive molecular dynamics (RMD) simulations based on the ReaxFF force field to investigate the mechanisms of the oxidation process of [001]-oriented pristine cylindrical Fe NWs with and without a C coating in an O_2 environment in order to obtain detailed insights into the influences of the surface C coating on the oxidation process at room temperature. Here, we show that the C-coated shell layer on the free surface of pristine Fe NWs partially controls the spontaneous oxidation when exposed to O_2 molecules by hindering the absorption–dissociation of O_2 molecules and diffusion of O ions into the shell layer. In particular, the surface modification of the pristine Fe NW with the C-coated shell layer has pronounced effects on the improvement of oxidation resistance by lowering the surface reactivity, which limits the formation of an oxide shell layer on the free surface of the NW. The formation of strong Fe–C bonds in the C-coated shell layer largely restrains the oxidation process. Furthermore, to examine the influence of the C-coated shell layer on the resulting modulation of mechanical properties of the pristine Fe NW, we systematically investigate the mechanical deformation processes and related properties of Fe NW with and without a C coating including their oxidized counterparts subjected to both uniaxial tensile and compressive loads at room temperature. The yield stress and strain (the elastic limit) of Fe NWs including the elastic and plastic deformation phase of the stress–strain relationship are found to be sensitive to the loading modes, the existence of the C-coated shell layer and the resulting formation of an oxide shell layer on the surface of the C-coated Fe NW.

Received 26th October 2021,
Accepted 29th October 2021

DOI: 10.1039/d1nj05108c

rsc.li/njc

1 Introduction

Oxidation of the reactive metallic materials and their alloys associated with corrosion is one of the longstanding problems in both materials science and nanotechnology.[1–9] Oxidation challenges their use and performance in a wide variety of chemically harsh oxidative reactive environments such as atmospheric exposure and chemical conditions.[1–11] The phenomenon exhibits a dramatic impact on the mechanical properties and eventually stability and reliability of the structural materials. Because of the high surface reactivity and especially high oxygen affinity, reactive metallic materials rapidly oxidize in reactive oxidizing environments where a thick oxide the shell layer completely, covering the free surface of reactive materials.[1–4,12–20] Unfortunately, the oxidation process detrimentally affects materials properties such as corrosion, loss of functional properties, and reduction of mechanical strength, which leads to unpredictable failure in mechanical loadings and particularly leads to significant financial loss.[1–6,8–15,18,20]

Fe and its alloys including their oxidized counterparts have been receiving significant interest for a broad range of potential applications in disparate fields including science, engineering, and technology as diverse as environmental remediation, magnetic imaging, catalysis, *etc.*, due to their excellent magnetic, mechanical, physical and chemical properties.[1–14,21–28] However, these materials undergo spontaneous oxidation with the formation of an oxide shell layer on their free surface when subjected to oxidizing environments such as exposure to O_2 molecules in the atmosphere. Therefore, a protective coating on the free surface is necessary to overcome this problem.[7,10–14,16,17,23] Unfortunately, the effects of relatively large surface-to-volume ratio and high oxygen affinity make Fe NWs susceptible and vulnerable to environmental effects.[2,6,7,10,23,24] Spontaneous surface oxidation is still considered as a major limitation for their applications.[6,9,19,26] Therefore, how to prevent the oxidation process, *i.e.*, oxide shell layer formation, is of interest in

[a] *Department of Physics, Izmir Institute of Technology, Urla, Izmir, 35430, Turkey*
[b] *Department of Mechanical Engineering, Wayne State University, 5050 Anthony Wayne Drive, Detroit, MI, 48202, USA*

their nanoscale applications.[4–6,9,24] In particular, the Fe NWs exhibit relatively higher chemical reactivity compared to their bulk counterparts and moreover, the influence of surface oxide on the mechanical properties becomes quite significant and plays important roles in determining their target performance.[9,10,12–14] Therefore, a detailed understanding including obtaining atomic-scale insights into the oxidation process of Fe and its alloys in a chemically reactive environment is an important, at the same time, technologically challenging problem.[6–14,23,24] The formation of an oxide shell layer on the free surface of Fe NWs results in a drastic change in the material properties and consequently plays an important role in the performance, functionality, and reliability of the Fe NWs that becomes more pronounced with the decreasing size of NWs.[2,3,7,10,24] For example, our previous simulations revealed that the pre-oxide shell layer has large effects on the mechanical deformation mechanism and related properties of metallic Fe NWs such as elastic strength.[12–14,18,29] Thus, the oxidation of the metallic Fe NWs is the main concern in their practical applications.

Generally, various types of surface coatings on the metallic Fe NWs have attracted particular interest in order to improve their physical, mechanical, catalytic, and chemical performance and properties.[2,5–11,22,25,27,28] The development of strategies to form antiferromagnetic oxide layers on the free surface of Fe NWs to reduce the negative impact of oxidation warrants a detailed atomic-level investigation.[2,5] The surface additional coating, *e.g.*, the surface passivation, of Fe nanomaterial is an effective solution to overcome surface oxidation.[4,8,9,27] In practice, carbon has been used widely in Fe materials to improve their mechanical strength and corrosion resistance, due to the outstanding properties stemming from the intermetallic reactions between Fe and C atoms.[6,8,9,11,27,28] Thus, to overcome the oxidation problem, based on the previous studies, it can be expected that the C coating on the surface of the Fe NWs as evidenced by well-known phenomena such as carbonization can provide an effective protection to inhibit oxidation and corrosion in reactive environments.[11,27] In addition, the encapsulation of Fe NWs with 0C atoms could also be of interest for corrosion resistance in magnetic and electrocatalytic applications such as magnetic imaging, magnetic recording media, catalysis, clean fuels and magnetic nano sensors.[2,8,9,27,28] In general, different approaches have been applied for the synthesis of C coatings on the pristine Fe nano-materials and their oxidized counterparts that introduce new properties in magnetic core Fe and oxidized-Fe materials in their applications.[2,6,23,29–31] Importantly, the surface coating of pristine Fe nanomaterials and their oxidized counterparts with different materials such as C has attracted a great deal of attention in functionalizing them simply by adjusting the size, shape, and shell thickness.[2,6,23,29–31] For example, the C-coated (-encapsulated) Fe nanoparticles have some specific properties and effects, and have been widely used in many fields of science such as application in the areas of nano biotechnology used in the fields of cancer treatments, magnetic resonance imaging [MRI], gene therapy, target-specific drug delivery, and many more.[6,23] Hydrophilic C coatings on the Fe_3O_4 nanorods, NWs, and nanoparticles protect them from oxidation and also improve mechanical and electrochemical properties such as superior electrical conductivity and stability as compared to bare Fe oxide counterparts.[32] For example, Garcia *et al.* reported a solution-phase strategy for depositing ultrathin graphene-like C onto Fe oxide nano-crystals (NCs) for corrosion resistance in magnetic and electro-catalytic applications.[30] Bae *et al.* reported the synthesis of C-coated Fe oxide (Fe_3O_4) nanoparticles by a hydrothermal method for use as contrasting agents in MRI.[31] Recently, many experimental researchers have focused on a surface C coating of the metallic Fe materials for specific target applications using the hydrocarbon radical precursors such as CH, CH_2, and CH_3 and/or CO and CO_2, mostly aiming to control the surface oxidation and corrosion, catalytic activity, and so on.[29,30,33] Importantly, the growth of the C shell layer depends strongly on the precursors used.[29] Specifically, the pristine Fe surface is coated (carburized) using CO molecules by three consecutive processes, *i.e.*, adsorption, dissociation of CO molecules on the Fe surface, and surface-to subsurface diffusion of C between 700 and 1100 K. However, the interaction of C-coated Fe NWs with O_2 is an extremely complex process, resulting in a gain and/or loss of some functional properties, but it is of more potential interest in mechanical reliability, environmental stability, corrosion protection and catalytic performance.[9,27,28] Therefore, comprehensive investigation of the C coating performance on the oxidation and mechanical deformation properties of the Fe NW is of great interest and a challenging issue for their technological applications.[11,28] Herein, a major challenge is to understand to what extent the free surface C coating is associated with the oxidation process on the Fe NW surfaces in an O_2 environment as well as the mechanical deformation behaviour and related properties of the Fe NWs using MD simulations based on a ReaxFF reactive force field. In particular, our aim is to investigate systematically how the surface C-coated shell layer provides specifically effective protection to the metallic Fe NW in an O_2 environment and how the C-coated surface modifies the deformation mechanism and related properties of Fe NWs under tensile and compressive loads.[11,28,34]

Although there are several studies that delineate the effect of coatings on the mechanical properties, such influences have not been investigated in the context of Fe NWs. Given the importance of Fe NWs as a structural component, we believe it is critically important to investigate such effects using a detailed molecular level approach. The capability of the ReaxFF method for describing the involved complex chemical processes makes the study a novel one. The ReaxFF, being the state-of-the-art-reactive potential with variable charges, has proven to be an efficient way and powerful method to study the effects of oxide shell layers on the mechanical properties of metallic NWs. The ReaxFF method has demonstrated its capability in predicting mechanical properties under externally applied mechanical loads on aluminium (Al), nickel (Ni) and Fe NWs.[11–15,18,20,34,35] Herein, we carried out MD simulation using the ReaxFF force field for Fe/C/O/proposed by Islam *et al.* that describes adequately the entire range of interactions among Fe/C/O atoms including

the coexistence of metallic, ionic, and covalent interatomic bonding.[11] Thus, it accurately reproduces experimental data for a wide range of physical, chemical, and mechanical properties of Fe/C/O/systems. In particular, it enables treating and computing correctly the non-uniform electron distributions in chemical reactions that incorporates with the local environment of each atom including dissociation, breaking, transition, and formation of chemical bonds in a consistent way in MD simulations.[11,34] The underlying mechanisms elucidated in the study will help develop further understanding on the behaviour of C-coated Fe NWs and will guide experimental synthesis of such NWs as well.

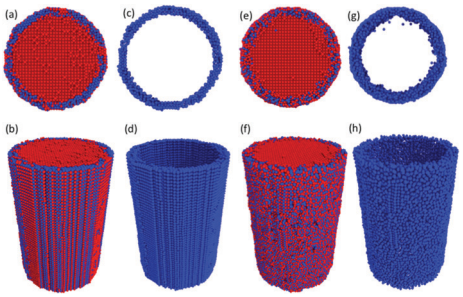

Fig. 1 Snapshots show the initial configuration of the C-coated Fe NWs: (a) side view and (b) axial view before and (e) side view and (f) axial view after the heat treatment. The blue and red spheres represent C and Fe atoms, respectively. For clear illustration, only the C atoms (blue) are shown in (c and d) before and (g and h) after annealing, while the Fe atoms in the core of the NW are hidden. Comparing (a–d) and (e–h), a total of 16 800 C atoms are randomly distributed around the free surface of metallic Fe NWs after the heat treatment.

2 MD simulation strategy and setup details for the oxidation process and mechanical deformation

The simulation methodology used in this paper is similar to that outlined in our previous works.[12–14,18,35] Here, we briefly describe the procedure for preparing the core–shell structure of C-coated cylindrical Fe NWs. The unit cell of the body-centred cubic (BCC) structure of the Fe lattice (lattice constant a = 2.863 Å) is replicated 70 × 70 × 50 times along the x, y, and z-directions, respectively. The [001]-oriented cylindrical NW is created by removing all atoms in the x–y plane at a distance greater than 5.0 nm from the centre of a rectangular box. The simulation cell contains 95 050 Fe atoms with the dimensions of 20.041 × 20.041 × 14.315 nm along the x, y, and z-directions, respectively. The length of the NW is aligned along the [001] direction, and sufficient vacuum space is included around it for inserting O_2 molecules.

To study the influence of the C coating on the oxidation process and on the mechanical deformation mechanism and related properties, we created an approximately 1.0 nm thick C coated shell layer on the free surface of pristine Fe NWs. The initial structure of the coating is created *via* replacing Fe atoms at the centre of the BCC unit cell with C atoms. The total number of C atoms is 16 800, which is approximately ∼17.6% of the total number of atoms. The C-coated NW (Fe/Fe_xC_y) is then relaxed using a conjugate gradient minimization scheme and then 300 K equilibration simulations are carried out for 100 ps. Next, we performed high temperature annealing simulation in order to make the structure amorphous. The NW is heated from 300 K to 1400 K and then maintained at the temperature for 100 ps followed by cooling down to 300 K. All heat treatment processes were performed using a canonical ensemble (*NVT*) using the Nośe–Hoover thermostat ensemble.[36] The high temperature heat treatment ensures structural reconstruction, which allows the atoms to occupy the energetically favourable positions. We calculated the radial distribution function (RDF) of the as created structures to assess the amorphous nature of the coating. Snapshots of the relaxed C-coated Fe NWs are shown in Fig. 1(a–d) and (e–h) before and after the heat treatment processes, respectively. Our atomic snapshots are visualized using the OVITO tool.[37] The snapshots provide clear evidence of the structural amorphization of the Fe_xC_y coating on the NW. The C atoms are found to be randomly distributed around the free surface of the NW rather than being in highly ordered orientation. Finally, the amorphous C-coated NW is used for the subsequent study to explore mechanical deformation mechanisms.

Next, we randomly placed 5000 O_2 molecules in the vacuum region of the MD box maintaining a gap of 0.6 nm from the free surface of the C-coated NW and its pristine counterpart. All oxidation simulations are performed using the canonical (*NVT*) ensemble at a temperature of 300 K.[36] The O_2 molecules are allowed to undergo the oxidation process and we observed atomic rearrangement of the surfaces of the NW due to interaction with the O-atoms. In the final step of the oxidation process, we removed all the O_2 molecules that did not interact with the C-coated Fe NW and its pristine counterpart.

The as prepared oxidized C-coated Fe NW as well as unoxidized counterpart is further equilibrated using a Nośe–Hoover isothermal–isobaric (*NPT*) ensemble at T = 300 K and zero pressure along the z direction.[38] The relaxed structures were then used for mechanical deformation simulations. We applied an external uniaxial uniform tensile and compressive loading at a constant strain rate of 1×10^8 s^{-1} along the axial z direction of the NWs to study the mechanical deformation process and related properties. Periodic boundary conditions were imposed in the axial (z) direction to avoid finite length of NWs. During all simulations, a velocity Verlet integrator with a time step of 0.25 fs is employed to update the atomic positions and velocities.[39] The charge equilibration is performed at each time step. Engineering atomic stresses are calculated using the virial theorem, as used in our previous MD studies.[39] We continued the tensile and compressive loading until the strain reached about ∼16% and ∼14%, respectively. Other relevant studies for the pristine and C-coated Fe NWs and their oxidized counterparts are performed under similar conditions of temperature, and constant strain rate. We carry out all MD simulations using the Large-scale Atomic/Molecular Massively Parallel Simulator (LAMMPS) package code.[40]

3 Results and discussion

3.1 Effect of carbon coatings on the oxidation process of the pristine Fe NW

It is of great importance to develop understanding in how and to what extent the existence of a C-coated shell layer affects the oxidation process of the pristine Fe NW. However, the atomic-scale oxidation process of the C-coated Fe NW, as compared to the pristine Fe NW, is a considerably complex process as the addition of the C atoms introduces an additional degree of complexity in the process. In order to evaluate the effectiveness and performance of the C-coated protective layers in the oxidation, we have performed a series of large-scale oxidation simulations of Fe NWs with and without C coatings. Here, the oxidation of the pristine Fe NW is used as a reference for further comparisons. We used an *NVE* ensemble at a temperature of 300 K for 0.5 ns.[36] The Fe NW with and without a C coating is exposed to an O_2 environment, containing randomly oriented 5000 O_2 molecules in the inserting volume of the MD box to allow for the oxidation process, as shown in Fig. 2. Periodic boundary conditions were implemented in all three directions.

We begin with a brief explanation of the oxidation process of the pristine Fe NW. Further details can be found in our previous works.[12] Fig. 2 and 3 highlight the time evolution of the total number of O uptake associated with the surfaces of pristine and C-coated Fe NWs, which reveals the kinetics (*e.g.*, the oxide shell layer evolutions) of the oxidation process. The oxidation of the pristine Fe NW in an O_2 environment occurs simultaneously *via* the dissociation and adsorption of O_2 molecules, and the inward diffusion of the O into the metallic core and the outward diffusion of the Fe ions through the growing oxide shell layer, subsequently leading to the formation of a thin oxide shell layer. At the initial stage of the oxidation, we observe high growth rates of the oxidation layer associated with the unbalanced diffusion rate of Fe and O atoms resulting in the formation of a shell (Fe_xO_y) layer due to the absence of rate-limiting barriers.[12,16,17] As the oxidation process continues, the continuously outwardly diffused Fe atoms react with the inwardly penetrated O ions, causing the oxidation of the pristine Fe NW and enlargement of the NW radius. The rate of the oxidation, dissociation activity, and O ion penetration rate decrease gradually because the diffusion paths of O ions are blocked by the continuing formation of the Fe_xO_y shell layer. Gradually, the presence of the dissociated and adsorbed O_2 molecules, *e.g.*, the developing oxide layer, on the free surface of NWs causes a reduction in the number of available surface sites for further reactions with the O_2 molecules, thus protecting the metallic core of the Fe NW from further reactions with O_2 molecules.

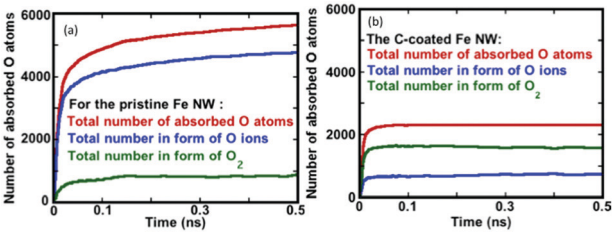

Fig. 3 The total number of O atom uptake associated with the incorporation of O_2 molecules and O ions with the (a) pristine and (b) C-coated surface of Fe NWs during the oxidation process at 300 K. Furthermore, the total number of O atoms (red), the total number of O atoms in the form of O ions (blue), and the total number of O atoms in the form of O_2 molecules (green) associated with the free surface of NWs are shown, respectively. The oxidation process of the C-coated Fe NW completed approximately by 0.07 ns.

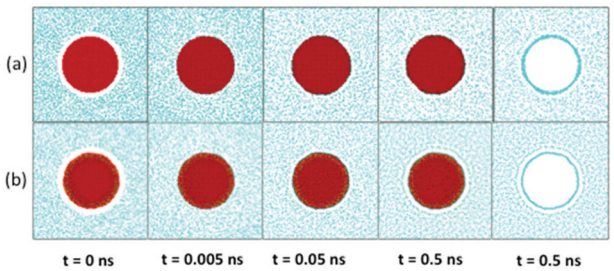

Fig. 2 Cross-sectional snapshots of the initial structure and the evolution of oxide shell layer formation on the free surface of the [001]-oriented (a) pristine Fe NW and (b) its C-coated counterpart are shown, respectively, at time = 0.0, 0.005, 0.05 and 0.5 ns. All NWs are initially inserted in a randomly distributed 5000 O_2 molecular environment. The red, cyan and yellow atoms are Fe, O and C, respectively. Additionally, for a better visualization to show the uptake of O atoms at the free surface of NWs, Fe and C atoms were hidden from the snapshots at the end of simulations. The formation of the surface oxide shell layer depends on the nature of the free surface structure.

As for the C-coated Fe NW, once the O_2 molecules reach the free surface of the NW, the oxidation reaction occurs relatively rapid. The beginning of oxidation is likely due to the dissociation and adsorption of O_2 molecules into the C-coated Fe lattice through O_2–C and/or O_2–Fe coupling. Adsorption describes the process of an O_2 molecule getting attached to the surface of the NW if the pair distance of O_2–Fe and/or O_2–C is equal to and/or less than 2.5 Å and 3.3 Å, respectively. Our result suggests that in the initial oxidation process, almost all O_2 molecules are close to the free surface that interacts directly with the C and Fe atoms around the C-coated shell layer and incorporate with Fe and C atoms on the preferential active adsorption sites around the free surface of the NW. Primarily, the cylindrical configuration of the C-coated Fe NW has a highly irregular surface and a complex atomic structure that provide a superfluous amount of active sites available for O_2 molecules to react with the C-coated Fe NW at the initial stage of oxidation, leading to an anisotropic dissociation and adsorption of O_2 molecules. However, a competition occurs between the dissociation and adsorption of O_2 molecules coupling (as bonding) with the surface Fe and C atoms. The oxide formation and growth process in an O_2 environment is driven by local reactions taking place around the available reactive free surface that evolve independently one from the other. As the oxidation process proceeds up to $\sim$0.07 ns, the resulting formation of an inhomogeneous and relatively thin $Fe_xC_yO_z$ oxide layer covers the free surface. The quick growth of the thin oxide layer with a

"limiting" thickness on the free surface of NWs including its resulting incorporation with the C-coated layer acts as a protective barrier and hinders the subsequent oxidation process. Nature of the relatively thin oxide layer formed on the C-coated surface of the NW can be related to its protectiveness of the NW against the oxidation process in an O_2 environment. Specifically, the thin oxide layer on the C-coated surface of the NW assists in strongly repelling the O_2 molecules and keeping them away from the free surface of the NW. Fig. 2 and 3 further indicate that most of the absorption and dissociation of O_2 molecules occur and distribute mainly on the free surface of the C-coated Fe NW. As a result, the corresponding metallic core dimension of the C-coated Fe NW does not undergo an apparent change after the oxidation process.

The interaction of O_2 molecules with Fe NW surfaces with and without a C-coating is of more general interest, and great importance for understanding the initial steps in the oxidation process, since the adsorption and dissociation of O_2 are believed to be essential for the formation of an oxide shell layer. Therefore, we investigate the details of time evolution of the oxidation process of the Fe NW with and without a C-coated shell layer by monitoring the total number of O atoms including the number of absorbed O_2 molecules and O ions that make direct bonding between the Fe and/or C atoms around the free surface of the NW during the oxidation, as shown in Fig. 3. In the initial stage, O_2 molecules quickly interact with the pristine Fe NW and its C-coated counterpart so that the surface is instantly oxidized. Comparison of the total number of O atom uptake associated with the incorporation of O_2 molecules and O ions with pristine (Fig. 3(a)) and its C-coated counterpart (Fig. 3(b)) surfaces of Fe NWs shows spontaneous oxidation at the free surface of the NWs, but exhibits a quite different characteristic for the pristine Fe NW and its C-coated counterpart. For example, a total of 5643 and 2318 numbers of O atoms are consumed at the end of the oxidation process (t = 0.5 ns) for the pristine and C-coated Fe NWs, respectively. Furthermore, the total number of O atoms in the form of O ions and O_2 molecules associated with the free surface of the pristine NW at the end of t = 0.5 ns is 4765 and 878, respectively. The corresponding numbers are 732 and 1586 for the C-coated Fe NW ($Fe–Fe_xC_yO_z$). This result reveals that the presence of the C-coated shell layer has a strong influence on the adsorption and subsequent dissociation of the O_2 molecules. Furthermore, the oxidized layer region on the free surface of the pristine NW contains mainly O atoms in form of O rather than O_2 molecules. In contrast to the pristine NW, the total number of O atoms in the form of O_2 molecules preferentially exists in the oxidized shell layer region of the C-coated Fe NW. This result reveals that the O_2 dissociation reaction becomes more unfavourable at the C-coated Fe NW surface. Also, the limited surface activity of the C-coated NW causes the formation of a relatively thin oxide shell layer, which passivates and prevents the C-coated surface from further oxidation; on the other hand, it causes to yield "limiting" thicknesses of the oxide layer as compared to its pristine counterpart.

Overall, we observed that the oxidation reaction between O_2 molecules and the free surface of pristine and C-coated Fe NWs mainly involved two consecutive processes, (i) adsorption and dissociation of O_2 molecules on the free surfaces, followed by (ii) the diffusion of the dissociated O ions towards the core of the NW, which consequently leads to the formation of a thin oxide layer. The number of adsorbed and dissociated O_2 molecules increases rapidly at the beginning stage of oxidation and then decreases dramatically with time for all the NWs. After the initial oxidation of the pristine NW, the total number of O atoms including the adsorbed O_2 molecules and dissociated O ions still decreases steadily due to the formation of a thin oxide shell on the free surface of the NW. But, the total number of O uptake associated with the adsorbed O_2 molecules and O ions on the C-coated surface changes rapidly at the initial stage of oxidation and quickly reaches a maximum at $\sim$0.07 ns. Then, it becomes almost constant thereafter, as shown in Fig. 3(b) because the formation of a relatively thin oxide layer on the free surface of the C-coated NW inhibits the interactions of O_2 molecules further. Interestingly, the fast increase of growing O atom concentration at the outer surface of the C-coated Fe NW results in a dramatic decrease in the oxidation rate by an increased activation barrier for adsorption and dissociation of O_2 molecules (the kinetic barriers for oxygen adsorption) on the C-coated surfaces compared to the pristine metallic surfaces.

We can conclude that the resulting formation of strong bonding between Fe and C atoms in the C-coated shell layer significantly impedes the incorporation of O_2 molecules on the free surface of the C-coated Fe lattice, the diffusion of the O ions into the C-coated shell layer, and the formation of an oxide shell layer. Each Fe atom located initially at each centre of the unit cell of BCC structure of Fe lattice was replaced by a single C atom. Therefore, the C–Fe bond length in these initial configurations is $\sim$2.47 Å. Then, it was allowed to relax until the C-coated crystalline Fe NW structure ($Fe–Fe_xC_y$) reached a configuration of minimum energy at 300 K using a conjugate gradient algorithm. After the relaxation as well as the heat treatment, the C–Fe bond length is found to be around at a distance of $\sim$2.00 Å, which is much shorter than the initial bond distance. Namely, these strong bonds lead to the shrinkage of interatomic distances. Also, the contraction of the Fe–C bond length causes significant distortion and strains on the local microstructure of the C-coated Fe NW in the radial direction after the relaxation with the heat treatment. Thus, the average diameter of the C-coated Fe NW decreases from $\sim$5.0 to $\sim$4.85 nm. The reason for the promotion of the oxidation resistance is that the strong interaction between Fe and C atoms in the layer on the surface of NWs inhibits the segregation of Fe and C from the surface and the formation of defects such as vacancies on the surface of the NW. Here, based on the above analysis, the surface C coating is an important means to partially protect the pristine Fe NW from the reactive O_2 environments. Modification of the free surface properties by C atoms makes the pristine NW relatively less reactive towards the O_2 molecules and thus prevents the further progression of the oxidation process. In particular, the surface C coating significantly affects the adsorption and dissociation of O_2 molecules on the surfaces of NWs and the inward diffusion

of the O ions deeper inside the metallic core of the C-coated NW plays an important role in the subsequent oxidation process.

Our current findings are consistent with the observations of the C shell layer encapsulating reinforced metallic Al nanoparticles (ANPs). Hong *et al.* studied Al/C interactions using ReaxFF to investigate the role of the C coating in the oxidation of bare ANPs using hydrocarbon precursors.[19] They demonstrated that the C coating shell layer was formed on the free surface of the pristine ANPs. Their results revealed that the C coating layer effectively served as a protective layer against oxidation only at low temperature in an O_2 environment. But the C coating layer was removed from the free surface at elevated temperatures, which makes ANPs very susceptible to oxidation.

3.2 Effects of the C-coated shell layer on the formation of the oxide layer

We analyse the details of the resulting oxide shell layer using the average radial atomic number density distributions of Fe, O, and C atoms per unit volume with a 0.5 Å radial bin size. Fig. 4 and 5 reveal the significant differences in the density of O atoms, the formation of an oxide shell layer, the penetration depth of O ions for the pristine NW, and its C-coated counterpart after exposure to O_2 molecules until 0.5 ns. The oxidation proceeds continuously through collectively inward O ion and outward Fe ion diffusions within the developing oxide shell layer on the pristine NW, resulting in an increased thickness of the oxide layer formation (Fe_xO_y). At the end of the oxidation process at t = 0.5 ns, a total of 5643 O atoms were consumed to form the oxidation layer (Fe_xO_y) on the free surface of the pristine NW where the oxidation rate correlates with the consumption of O ions. Importantly, the initial relaxed crystalline structure of the free surface of the pristine NW as seen in Fig. 4(a) has undergone substantial alteration such as local structure of the surface and atomic charge states of atoms around the active sites of the free surface as a result of the corresponding ionic diffusion of species during the oxidation process. Thus, the average diameter of the pristine NW is increased from r = ~5.0 to ~5.2 nm, which is equivalent to ~11% volume expansion of the pristine NW with an ~1.7% increase of NW weight, as shown in Fig. 4(b). The volume expansion of the pristine NW can be clearly seen from the decrease in the average radial number density of the Fe atoms after the oxidation, as compared to Fig. 4(a) and (b). The calculated

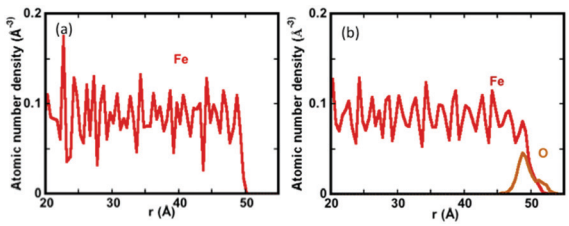

Fig. 4 The average radial atomic number density profiles of Fe (red) and O (brown) atoms per unit volume for the relaxed structure of the initial pristine Fe NW (a) before and (b) after the oxidation process, respectively.

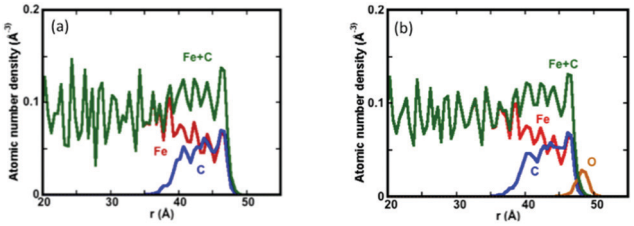

Fig. 5 The radial density profiles of Fe (red), C (blue), O (brown) and Fe + C (green) atoms per unit volume for the relaxed structure of the C-coated Fe NW (a) before and (b) after the oxidation process (t = 0.5 ns), respectively. Notably, the profiles reveal that the average diameter of the C-coated NWs shrunk slightly inward of NW. The total O atom number in the oxide region for the oxidized C-coated Fe NW ($Fe–Fe_xC_yO_z$) is 2318.

average radial number density of O atoms shows a peak in Fig. 4(b), which is correlated with the thickness of the oxide layer on the free surface. The position and intensity of the peaks reveal that the resulting oxide layer on all the NWs remains highly non-uniform, depending on the depth of the NW and indicating limiting diffusion behaviour.

Initially, the 16 800 C atoms were inserted *via* replacing Fe atoms within around ~1.0 nm thickness of the NW surface. After the high-temperature heating, the initial uniformly distributed C atoms undergo substantial reconstruction and the ordered structure disappears. For example, the C atoms diffuse to stable sites from the region with high C concentration to that with low concentration during the high-temperature heating process, degrading the crystallinity of the Fe NW to some extent. The heat treatment leads to the broadened C atom segregation domains and consequently the changes of the pre-existing defect structure within the C-coated layer. It indicates that the randomly distributed C atoms occupy a significant portion of the NW as compared to the pristine counterpart as shown in Fig. 5(a). Therefore, the high temperature heat treatment process results in a significant rearrangement of C atoms around the free surface of NWs that consequently changes the initial distribution of radial spatial number density of C atoms, due to penetration of C atoms into the metallic core of NWs. Importantly, the average diameter of the C-coated NW shrunk slightly from ~5.00 to ~4.85 nm after the heat treatment and relaxation processes.

Fig. 5 highlights the O atoms incorporated with the C-coated Fe NW and the formation of the resulting oxide layer that continuously degrades the surface related physical and chemical properties such as the pre-existing defects and diminution of mechanical properties of the NWs. The C-coated NW (Fig. 5) experienced slight radial expansions as a result of the oxidation process, where the radial number density of the initial Fe and C atoms decreases insignificantly as compared to the oxidized counterpart (Fig. 5). It implies that the surface Fe and C atoms are not mobile within the developing oxide layer. At the end of the oxidation process at t = 0.5 ns, the radial average number density distribution of O atoms has a relatively small peak around the reactive region of the free surface of NWs. The position, width and intensity of peaks indicate that a small amount of O penetrates underneath the C-coated shell layer, and mostly remains on the free surface. This result implies that the C-coated layer creates a

resistance against the inward diffusion of O ionic species to react with the metallic core of the NW.

Analysis of the radial atomic number density of O atoms per unit volume suggests that the C-coated layer strongly influences the penetration depths of O ions and the formation of the oxide layer primarily associated with the inward diffusion of O ions that are much larger for the pristine NW. We demonstrate that the C coating is responsible for introducing additional resistance for the diffusion of O ions as well as their mobility by preventing the pathways for ionic movements. Initially, the coating isolates partially the direct contact of O_2 molecules from the pristine Fe NW and/or hinders the formation of a direct path for O and Fe ion movement, overall causing an increase in the oxidation resistance of the NW.

Our current findings are consistent with the observations for the encapsulating C shell layer reinforced metallic Fe nanoparticles (NPs). Tavakkoli *et al.* observed that the encapsulating C shell layer protects the Fe NPs from oxidation in air.[41] Specifically, the single C shell layer does not prevent desired access of the reactants to the vicinity of the Fe NPs but protects the active metallic core from oxidation. However, the multiple C shell layers hinder desired access of the reactants to the Fe core, thus adversely affecting the catalytic activity of the Fe NPs.

3.3 Structural properties of the C-coated Fe NW and its oxidized counterpart

Here, we perform detailed characterization of the spatial short-range local microstructural properties and correlations including changes and arrangements of Fe–Fe and Fe–C atoms of the C-coated Fe NW after the heat treatment and oxidation process by RDF. The RDFs of Fe–C and Fe–Fe for the C-coated Fe NW are shown before (Fig. 6(a)) and after (Fig. 6(b)) the oxidation process. First, the C coating effects on the structural properties of the pristine Fe NW are investigated using the RDF of Fe–C pair. During the heat treatment process, the applied thermal treatment and relaxation processes are primarily responsible for the diffusion and segregation of C atoms in the metallic Fe NW to generate a C-coated shell layer (Fe_xC_y) on the NW surface. At the end of the heat treatment process, the existing C atoms are distributed randomly around the free surface of Fe NWs due to the atomic rearrangement, which forms a metastable (Fe_xC) phase. Hence, the overall average Fe–C bond length is ~2.00 Å, as seen in Fig. 6. The Fe–C bond length has been shortened compared to the initial position (*e.g.*, before the heat treatment), confirming the nature of attractive force between Fe and C atoms. Also, this indicates that the C-coated Fe surface has undergone substantial alteration and modification in some way to make it less reactive. As a result, the C atoms in the Fe NW are correlated with the substitutional incorporation of C atoms in the Fe lattice interstitial sites forming the Fe_xC carbide phase in good agreement with the crystalline Fe_3C phase.[42]

Similarly, to gain a better understanding of the resulting oxidation effect on the change in the structural properties and phase composition of the pristine Fe NW and its C-coated counterpart, we investigated detailed spatial short-range local structural correlations using the RDFs of the Fe–Fe, Fe–C, Fe–O and C–O bond lengths. The change of Fe–Fe and Fe–C bond length distribution of the C-coated Fe NW before and after the oxidation process is shown in Fig. 6(a) and (b), respectively. Importantly, the bond length of the Fe–C atoms in the C-coated Fe NWs is at ~2.00 Å before and after the oxidation. Moreover, prior to the oxidation, the RDF of the system (Fig. 6) shows that there are two peaks for the Fe–Fe pair at ~2.45 Å and ~2.83 Å in the C-coated region, corresponding to the atomic distance between corner and center Fe atoms, and between the corner of Fe–Fe atoms, respectively. Additionally, the first peak distribution in the C-coated NW is sharp. We note that the distribution of Fe–Fe atoms is also related to the thickness of the shell region. For example, we analyze the RDF of Fe–Fe of the C-coated Fe NW in the shell region in between 50–33 Å.

On the other hand, the first and second peaks in RDF for the Fe–Fe pairs occur at 2.50 Å and 2.75 Å, respectively, after the oxidation. Our results demonstrate that the oxidation process caused a slight change of the Fe–Fe bond lengths in the C-coated NW. But, the bond length of Fe–C atoms on the C-coated Fe NW layer remained almost unchanged. This analysis showed us that there are no significant changes to occur for the RDF of the Fe–Fe and Fe–C atoms around the surface region before and after the oxidation process. With respect to Fe–Fe pair interactions, Joan *et al.* also observed two similar peaks at 2.45 and 2.80 Å for the Fe(100) oriented surface at 900 K.[16] Based on the RDF of Fe–O for the C-coated Fe NW as clearly shown in Fig. 7(a), the nearest first peaks in the Fe–O pair split into two peaks, centred at ~2.0 and ~2.75 Å with different amplitudes. Similarly for the pristine Fe NW as shown in Fig. 8, the Fe–O bond length is located at ~1.6 and ~2.0 Å. Interestingly, the Fe–O bonding distance especially depends on

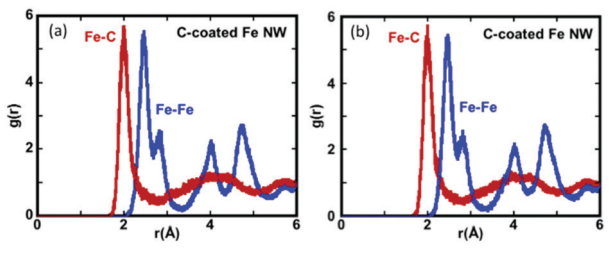

Fig. 6 Radial pair distribution function, $g(r)$, for Fe–C (blue) and Fe–Fe (red) for the relaxed structure of the C-coated Fe NW (a) before and (b) after the oxidation process in the shell region of 50–33 Å, respectively, before the applied mechanical loads.

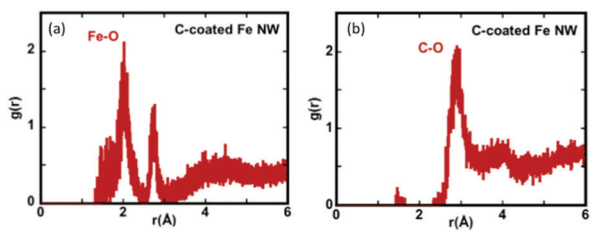

Fig. 7 Radial pair distribution function $g(r)$ for Fe–O (a) and C–O (b) atoms for the C-coated Fe NW in the shell region in 50–33 Å after the oxidation process.

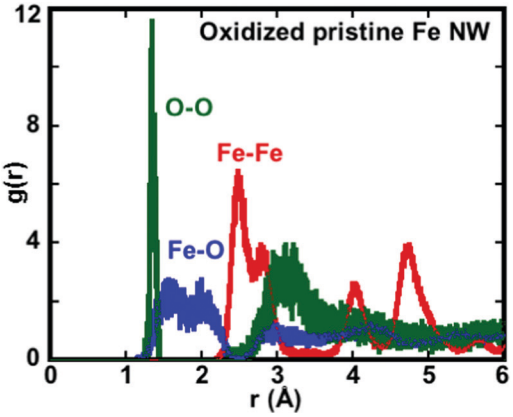

Fig. 8 Radial pair distribution function $g(r)$ for Fe–O (blue), Fe–Fe (red) and O–O (green) atoms for the pristine Fe NW in the shell region in 50–40 Å after the oxidation process.

the diffusion of O ions into the NW that significantly rearrange the surface of the Fe–O structure in the pristine Fe NW. Moreover, the RDF of O–O has a sharp peak with the maximum amplitude located at ~1.35 Å. The O–O peak presumably corresponds to the distances between the O atoms from the un-dissolved O_2 molecules at the oxide shell layer. The C–O bond length is just around ~1.43 Å in organic molecules.[43] The result for the first peak in RDF for the C–O distance at ~2.90 Å indicates an interatomic distance, where the O_2 molecule and O atoms are bound to Fe atoms, resulting in a minimal overlap of atomic orbitals at that distance by surrounding the C atoms. Importantly, our results indicate that the presence of C atoms around the free surface of Fe NWs affects significantly the bond length of Fe–O atoms.

The atomic distribution profiles indicate clearly (Fig. 2 and 3) that the C-coated Fe NW oxidizes by the incorporation of O_2 molecules and O ions through the absorption and partially dissociation of O_2 molecules on the surface of the C-coated NW. As a result, the corresponding C-coated NW surface does not undergo a substantial alteration after the oxidation process, where O_2 molecules get attached to the Fe NW free surface and O ions stay around the free surface of the NW. Hence, they do not contribute to significant changes in the structural properties of the C-coated NW because of the formation of only a thin oxide shell layer on the free surface. Thus, the segregation and reconstruction of C atoms around the free surface induce changes in the structural, chemical, and physical properties of the NW, consequently influencing the oxidation process and mechanical performance.

Furlan *et al.* investigated the characteristics of chemical bonds and structure of amorphous nanocomposites of iron-carbide ($Fe_{(1-x)}C_x$) thin films in a broad composition range by X-ray diffraction and high-resolution transmission electron microscopy (TEM) together with selected area electron diffraction and PDF analysis, X-ray photoelectron spectroscopy, Raman spectroscopy, and soft X-ray absorption spectroscopy.[42] Their results show that the amorphous region consists of two phases: (i) an amorphous carbide phase, and (ii) an amorphous carbon matrix. They observed that the PDF peak for the Fe–Fe bond distance is about 2.5 Å, implying the Fe–Fe bond length distance in the crystalline carbide (Fe_3C) phase that agrees well with our results.[42] Moreover, the second coordination shell distance of Fe–Fe is ~3.8 Å which agrees with that of the Fe_3C structure. They observed that the PDF peak for the Fe–C bond length is at ~2.0 Å that agrees well with our results.

3.4 The effect of the C-coated shell layer on the tensile and compressive strength of the NWs

We focus on the effect of the C coating with and without the presence of formation of oxide shell layers on the mechanical deformation and related properties of the Fe NW under the uniaxial tensile and compressive loadings. Here, we take the pristine Fe NW as a reference in order to compare to what extent the C-coated surface with and without an oxidized layer (*e.g.*, the surface modification) degrades and the mechanical deformation mechanism and the related properties of the NWs. All the studies were performed at T = 300 K using a constant strain rate of 1×10^8 s^{-1}.

Fig. 9 presents the evolution of engineering tensile stress–strain curves reflecting the effects of surface C coatings and resulting oxidation on the tensile properties and deformation mechanism compared to the pristine Fe NW. One can observe that the stress–strain profiles exhibit an initial elastic deformation stage; the flow stress increases linearly at first followed by the non-linear increment with the increase of strain up to the maximum stress level in the tensile elastic regime. Then, it undergoes a drastic drop in the value of yield stress as shown in Fig. 9, partially releasing the elastic energy (relieving tensile stress) by nucleating defects associated with the incipient tensile plasticity. The average yield stress to cause the onset of the tensile plastic deformation and the corresponding average yield strain values are ~8.25 and ~8.70 GPa and ~10.50 and ~9.72%, respectively, for the pristine and C-coated NWs as shown in Fig. 9(a). The tensile flow stress reaches a maximum value to cause the onset of tensile plasticity beyond which it drops abruptly down to ~−3 GPa and ~4.0 GPa for the pristine and its C-coated counterpart, respectively (see Fig. 9(a)). Consequently, it fluctuates around a certain stress value and a smoother tensile plastic response is observed for all NWs, suppressing the flow stress

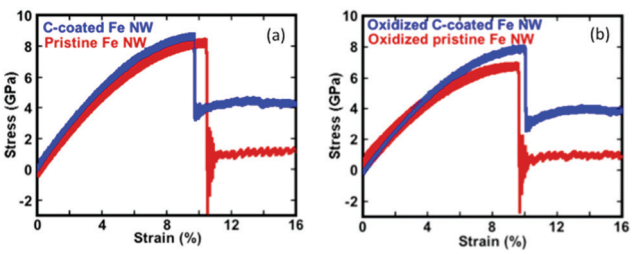

Fig. 9 Evolution of engineering tensile stress–strain curves (a) for the pristine and C-coated Fe NWs, and also (b) for their oxidized counterparts, respectively. Characteristic effects of the C-coated shell layer and the formation of an oxide shell layer on the deformation mechanism of the pristine NWs are shown under the tensile load.

value from further escalation. The existence of the C-coated shell layer slightly enhances the tensile yield stress to cause the onset of tensile plasticity, and also it increases the tensile flow stress during the plastic deformation, indicating the important role of the C-coated shell layer on the surface of the pristine Fe NW. Specifically, the engineering stress–strain curves in the tensile plastic region suggest that C-coated Fe NWs exhibit a relatively higher resistance in the plastic deformation regime.

Additionally, the average yield stress to cause the onset of the tensile plastic deformation and the corresponding yield strain values for the oxidized pristine and C-coated NW are ~6.80 and ~7.95 GPa, and ~9.60 and ~9.98%, respectively. The tensile plastic yield stress for the oxidized C-coated Fe NW is lower, but the corresponding elastic limits are slightly higher than those of its non-oxidized counterpart. Also, the tensile plastic deformation for the oxidized C-coated Fe NWs requires a higher stress value with the incipient tensile plasticity, *e.g.*, the repeated generation of new dislocations along twin boundaries with the increase of applied tensile strain compared to its oxidized pristine counterpart. Low tensile flow stress beyond a yield stress value leads to tensile plastic relaxation for all NWs with the nucleation of defects in the twin boundaries. Thus, our results reveal that the formation of an oxide shell layer on the NWs promotes activation of the initial dislocation nucleation associated with the inception of tensile plasticity.

Our results show that the C-coated surface with and without the existence of an oxide shell layer has a significant effect on the tensile yield stress and strain to cause the onset of the tensile plasticity, and overall tensile mechanical deformation behaviours. Firstly, the surface modification of pristine Fe NWs with C atoms distinctly enhances the yield stress level and expedites the nucleation of dislocations; thus, the tensile plasticity becomes relatively stronger. Likewise, the oxide shell layer causes earlier onset of tensile plasticity for the pristine NW. Also, the tensile elastic limit is reduced slightly by the presence of C atoms, but the oxide shell layer on the free surface of the C-coated Fe NW case increases it.

Despite similar tensile mechanical behaviour, the yield stress and strain values are changed by the existence of the C coating and the resulting oxide shell layer. The presence of defects related to the formation of the oxide shell layer provides easy pathways for initiation of dislocations to cause the onset of tensile plasticity. The amount of pre-existing defects is relatively more abundant in the oxidized C-coated Fe NW than its un-oxidized counterpart, thus exhibiting some differences in the onset of tensile plasticity and consequently corresponding mechanical properties. For example, the oxidized pristine and C-coated Fe NW possesses relatively low yield stress compared to the non-oxidized counterparts, suggesting that the occurrence of the oxidation process alters the structural properties and the existence of defects on the NW surfaces.

The evolution of engineering compressive stress–strain responses of the pristine and C-coated Fe NWs, and their corresponding oxidized counterparts is shown in Fig. 10(a and b). The figure suggests that the C coating and the formation of the oxide layer profoundly affect the compressive mechanical properties

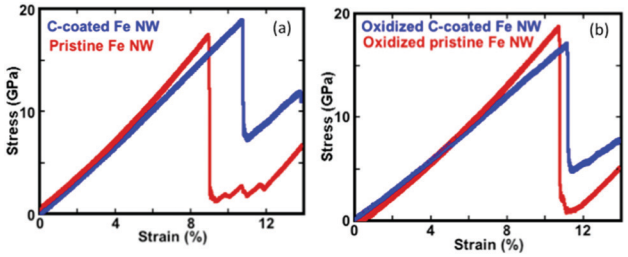

Fig. 10 Evolution of engineering compressive stress–strain curves (a) for the pristine and C-coated counterparts and (b) for their oxidized counterparts. Characteristic effects of the C-coated shell layer and the formation of the oxide shell layer on the deformation mechanism and related properties of the pristine NWs are shown under the compressive load.

such as the compressive yield stress and strain (*e.g.*, the elastic strain region) compared to the pristine NW. The compressive flow stress first increases linearly in the compressive elastic regime with the increase of strain up to the maximum stress level. Then, it follows a significant drop in the value of yield stress, relieving stress by nucleating dislocations in the surface that indicates the onset of compressive plasticity. The compressive elastic–plastic transformation, *e.g.*, the yield stress and strain to cause the onset of the compressive plasticity, occurs at ~17.5 and ~18.9 GPa, and the corresponding yield strains are ~9.0 and ~10.8%, for the pristine and C-coated Fe NWs, respectively. It indicates that the compressive yield stress value for the C-coated Fe NW is higher, and the corresponding compressive elasticity limit is larger than that of its pristine counterpart. Additionally, the average values of the compressive yield stress and strain for the oxidized pristine and C-coated Fe NW are ~18.6 and ~17.1 GPa, and ~10.75 and ~11.23%, respectively. It suggests that the oxidized pristine Fe NW exhibits a higher resistance to the onset of compressive plasticity than its corresponding C-coated counterpart.

Comparing the compressive stress–strain curves in Fig. 10, they exhibit higher sensitivity to the C-coated layer. The corresponding mechanical properties reveal some features such as the compressive yield stress and strain, the compressive elastic limit, and the compressive plasticity. The existence of C coatings contributes greatly to withstand the relatively high compressive strain caused by the compressive loading. Moreover, the C-coated shell layer leads to an increase in the plastic yield stress of metallic Fe NWs. Changing the surface composition and structural properties of C-coated Fe NWs as a result of the heat treatment process remarkably increases the elastic compressive limit and the yield stress to cause the onset of compressive plasticity. The stress–strain curves of the NWs indicate a significant influence of C coatings and oxidation on the subsequent compressive and tensile deformation performance and related mechanical properties of the pristine Fe NW. The yield stress and strain values to cause the onset of plasticity including both elastic and plastic strain have strong competition and correlations with the surface states that is related to the pre-existing surface defect structures, amount, and distributions as well as the type of external loadings.

Note that our results are consistent with the previous simulations and experimental literature. For example, Byggmastar *et al.* investigated the uniaxial tensile deformation mechanism

and related mechanical properties of cylindrical [001]-oriented Fe and iron–chromium (FeCr) NWs, including the effects of Cr content and size of the NW using MD simulation based on both an embedded atom method (EAM) and a Tersoff-like bond order potential (BOP).[44] For each case of the FeCr NWs, substitutional Cr atoms were randomly inserted in the NWs to get the desired concentrations between 0 and 20 wt%. The FeCr NWs are elastically softer and weaker than the pure counterpart, which was explained by the relatively weak Fe–Cr interaction, compared to the pure Fe–Fe interaction. For example, the tensile yield strength and ultimate strength decrease with increasing Cr concentration or the diameter. Similar to our results, the plastic deformation mechanism is mediated by twinning for both potentials at all studied Cr concentrations and diameters. Luu and Gunkelmann investigated the mechanical response of Fe–C single crystals and polycrystals under hydrostatic and uniaxial compression using EAM potential.[22] They concluded that the existence of C atoms strongly increases the Fe–C phase transformation pressure but decreases the elastic–plastic transformation and also the elastic limit. Xie *et al.* experimentally observed that the compressive strength of Fe nanopillars (with diameters of 150 nm and lengths of 450 nm) with low dislocation densities (pre-existing defects) was substantially stronger than with high dislocation densities, indicating that the initial dislocation density controlled compressive deformation.[45] For example, they observed that the plastic deformation behaviour of nanopillars containing high dislocation densities proceeds continuously or discretely *via* a series of small- and intermediate-scale strain bursts that were associated with the movement/escape of dislocations and the formation of slip bands. Li *et al.* investigated the effect and role of amorphous C coatings including the thickness of amorphous C coatings on the mechanical behaviour of [111]-oriented silicon carbide (SiC) NWs *via* using MD methods at room temperature.[46] They show that the amorphous C layer enhances the mechanical properties of SiC NWs, serving as a protective coating to shield the crack growth in the SiC NWs. Moreover, an amorphous C coating makes SiC NWs relatively more ductile and also, an increase of the coating thickness leads to a brittle-to-ductile transition for the NWs. Wei and Yu studied the effect of substitutional lithium (Li) atoms on the tensile mechanical behaviours of α-Fe including specifically the tensile stress–strain relationship and the tensile plastic deformation mechanism of the α-Fe single crystal with three different lattice orientations (*i.e.* [100], [110] and [111]) and five different Li concentrations (*i.e.* 0, 0.05, 0.1, 0.2 and 0.3%) using MD simulations based on the EAM in detail. The substitutional Li atoms were introduced into the system by replacing Fe atoms randomly.[47] Similar to our results, detailed dynamic characterization of all the tensile stress–strain curves clearly exhibits linear behaviour at the early stage of the tension and then nonlinear behaviour before the yield stress. They showed that the Li atoms influence significantly the tensile plastic deformation mechanisms and degrade the mechanical properties of the α-Fe single crystal. For example, the Young's moduli decline with the increase of Li concentration. The tensile yield stress declined monotonically for all the three orientations as the amount of Li atoms increased. The [111]-orientated crystal was more sensitive to the existence of Li atoms than the other two orientations. Importantly, the influence of substitutional Li atoms was insignificant for the [100]-orientated crystal. For example, the substitutional Li atoms slightly change the slopes of the stress–strain curves in the nonlinear elastic parts, *e.g.*, before the abrupt drop of the yield stress. Chen *et al.* systematically investigated the role and influence of the Ni concentration and temperature on the deformation mechanism and mechanical properties of BCC Fe–Ni alloy NWs with a diameter of 8.0 nm under tension loading along the [001] direction at a constant rate of 8×10^8 s^{-1} using MD simulations.[25] The Fe–Ni alloy NWs are obtained as follows: the substitutional Ni atoms were introduced into the system by replacing Fe atoms randomly. They found that the tensile deformation mechanisms of the Ni–Fe alloy NWs depend significantly on the Ni concentration. For example, the NWs with a low Ni concentration deform mainly by the twinning mechanism at low temperatures. Also, their results indicated that all NWs exhibit a similar stress–strain behaviour under uniaxial tension with a different elastic modulus. Moreover, they revealed that there was a significant linear relationship between the Ni content, temperature, and ultimate stress of the NWs. It was found that the local atomic pressure fluctuation of the Fe–Ni alloy NW surface became more prominent with an increase in the Ni content, which may serve as the defect for dislocation nucleation.

Sen *et al.* studied the influence of the O_2 oxidizing environment on the mechanical tensile properties of Al NWs under three different strain rates using RMD simulations.[15,20] They demonstrated that the oxidation process drastically changes the mechanical behaviour and properties of Al NWs as the surface-to-volume ratio increases which is in good agreement with our results.[15,20] For example, resulting formation of an ~1.0 nm thick amorphous oxide shell on the Al NW increases the ductility and decreases the strength (the decrease in the yield stress and also Young's modulus of Al NWs), where the oxide shell exhibits superplastic behaviour. Moreover, the oxide amorphous shell on the Al NW and the disordered atomic structure of the Al/AlO_x interface decrease the Al dislocation nucleation stress to cause the onset of plastic deformation by increasing the activation volume and the number of nucleation sites. Namely, the oxide shell and the core–shell interface can provide a defect nucleation site increasing the ductility of the Al NWs. Rosandi *et al.* investigated intensively the influences of oxide shell layer thicknesses on the tensile and compressive mechanical deformation behaviours of the Al NWs at different strain rates using RMD methods with a ReaxFF potential.[48] They revealed that the existence of the oxide shell layer (alumina coating) assists to increase the ductility of Al NWs without significant reduction in tensile strength, but the thickness of the coating is less decisive during compression. Godet *et al.* investigated the tensile mechanical properties of a crystalline [110]-oriented gold (Au) core–amorphous silicon (a-Si) shell NW, including the onset of plasticity at a constant strain rate using MD simulations with Modified Embedded Atom Method (MEAM) potentials.[49] Notably, they observed that the core–shell NW sustains relatively higher stresses with a homogeneous plastic deformation behaviour as compared to the pristine Au

NW. They noted that the onset of the plastic deformation in the core–shell appeared at smaller strain than in the pristine Au core alone at $T = 100$ K.

The surface states are predominantly related to the resulting formation of bonding between atoms and the pre-existing defects created upon the C coating and oxidation process. Also, the oxidized NW experiences changes in morphology and sizes, as well as the formation of numerous defects in the free surface of NWs that influence the tensile and compressive mechanical properties. For example, the presence of O atoms within the C-coated Fe NW leads to decreased compressive and tensile yield stress of the C-coated NW. Notably, encapsulation of the pristine Fe NW with C atoms results in lowering of the average diameter of the C-coated NW due to the stronger Fe–C interactions. According to previous studies, the mechanical properties of crystalline core/shell Fe NWs can be affected by the interactions between C and Fe atoms that cause the displacement of Fe atoms from the equilibrium position to form ''strained'' configuration of the Fe network in the C-coated shell layer and the generation of defects. Also, the replacement of C atoms in the surface of the pristine Fe NW naturally leads to a decreased number of dislocations sites and point defects as compared to the pristine counterpart. Moreover, the presence of O atoms within the pristine Fe NW and its C-coated counterpart destructs the Fe network connectivity and/or results in the lattice distortion and the structural heterogeneities (imperfections) that act collectively as defects to facilitate the onset of tensile plasticity. Thus, the lattice mismatch including dangling bonds at the interface between the core and shell, the intrinsic stress gradient of the NW, the disorder-induced distortions in the crystal/amorphous interfaces, interface boundary effect of the core–shell structure, and surface reconstruction help to change the physical and chemical characteristics of the NWs.[50]

4 Conclusions

We investigated a strategy to protect the pristine Fe NW from oxidation using a thin C coating. We used ReaxFF reactive MD simulations to study the effect of the resulting C-coated surface on the oxidation process of the pristine Fe NW at room temperature. We observed that the surface reactions of the pristine Fe NW have very different characteristics from its C-coated counterpart. Our results demonstrated that the limited formation of a thin oxidation shell layer on the free surface of the Fe NW is inevitable despite the existence of the C-coated layer. Also, we observed that the C-coated Fe NW has a relatively lower reactivity than the pristine metallic Fe NW. Namely, the strong bonds between Fe–C and interstitial C–C atoms in the C coating would greatly restrain the oxidation process, controlling the oxide growth and migration of O ions on the surface of the NW. For example, the C-coated layer on the free surface of the NW acts as an effective protective layer to significantly reduce the incorporation of the total number of O atoms including adsorption and dissolution of O_2 molecules as the oxidation process proceeds. Namely, the C-coated Fe NW is partially resistant to adsorption and dissolution of O_2 molecules on the free surface of the C-coated Fe NW as well as to the penetration of O ions underneath the C-layer to react with the metallic core of the Fe NW in an O_2 environment. Besides, the C-layer on the free surface of the pristine Fe NW as well as the resulting formation of an oxide layer has a significant effect on the mechanical performance and related properties such as the yield stress and strain of Fe NWs. Fundamentally, our results presented here reasonably suggest that the C-coated shell layer on the free surface of Fe NWs could be of practical interest and beneficial for a wide range of diverse practical applications.

Conflicts of interest

There are no conflicts to declare.

Acknowledgements

This work was supported by The Scientific and Technological Research Council of Turkey (TUBITAK)-BİDEB 2219 through Grant No. 1059B191400364. Simulations were performed at TUBITAK ULAKBIM, High Performance and Grid Computing Center (TR-Grid e-Infrastructure), and ITU National Center for High Performance Computing (UHEM). MMI acknowledges startup funds from Wayne State University.

References

1 T. Pan and Y. Lu, *Int. J. Electrochem. Sci.*, 2015, **6**, 4967–4983.
2 M. A. Zeeshan, S. Pané, S. K. Youn, E. Pellicer, S. Schuerle, J. Sort, S. Fusco, A. M. Lindo, H. G. Park and B. J. Nelson, *Adv. Funct. Mater.*, 2013, **23**, 823–831.
3 H. DorMohammadi, Q. Pang, L. Árnadóttir and O. B. Isgor, *Comput. Mater. Sci.*, 2018, **145**, 126–133.
4 I. P. Jamal, S. K. Chong, K. W. Chan, M. Othman, S. A. Rahman and Z. Aspanut, *J. Nanomater.*, 2013, 1–7.
5 D. Zhang, S. Wei, C. Kaila, X. Su, J. Wu, A. B. Karki, D. P. Young and Z. Guo, *Nanoscale*, 2010, **2**, 917–919.
6 I. P. Grudzinski, M. Bystrzejewski, P. Bogorodzki, A. Cieszanowski, W. Szeszkowski, M. Poplawska and M. Bamburowicz-Klimkowska, *J. Nanopart. Res.*, 2020, **22**(82), 1–17.
7 Y. P. Ivanov, A. Alfadhel, M. Alnassar, J. E. Perez, M. Vazquez, A. Chuvilin and J. Kosel, *Sci. Rep.*, 2016, **6**, 24189.
8 D. Dwivedi, K. Lepkova and T. Becker, *RSC Adv.*, 2017, **7**, 4580.
9 M. Fronczak, O. Labedz, W. Kaszuwara and M. Bystrzejewski, *J. Mater. Sci.*, 2018, **53**, 3805–3816.
10 M. Krajewski, K. Brzozka, W. S. Lin, H. M. Lin, M. Tokarczyk, J. Borysiuk, G. Kowalski and D. Wasik, *Phys. Chem. Chem. Phys.*, 2016, **18**, 3900–3909.
11 M. M. Islam, C. Zou, A. C. T. van Duin and S. Raman, *Phys. Chem. Chem. Phys.*, 2016, **18**, 761–771.

12 G. Aral, Y. J. Wang, S. Ogata and A. C. T. van Duin, *J. Appl. Phys.*, 2016, **120**, 135104.
13 G. Aral, *J. Appl. Phys.*, 2019, **126**(13), 135109.
14 G. Aral, M. M. Islam, Y. J. Wang, S. Ogata and A. C. T. van Duin, *Phys. Chem. Chem. Phys.*, 2018, **20**, 17289–17303.
15 F. G. Sen, A. T. Alpas, A. C. T. van Duin and Y. Qi, *Nat. Commun.*, 2014, **5**, 3959.
16 B. Jeon, Q. V. Overmeere, A. C. T. van Duin and S. Ramanathan, *Phys. Chem. Chem. Phys.*, 2013, **15**, 1821–1830.
17 R. Subbaraman, S. A. Deshmukh and S. K. R. S. Sankaranarayanan, *J. Phys. Chem. C*, 2013, **117**, 5195–5207.
18 G. Aral, M. M. Islam and A. C. T. van Duin, *Phys. Chem. Chem. Phys.*, 2018, **20**, 284–298.
19 S. Hong and A. C. T. van Duin, *J. Phys. Chem. C*, 2016, **120**, 9464–9474.
20 F. G. Sen, Y. Qi, A. C. T. van Duin and A. T. Alpas, *Appl. Phys. Lett.*, 2013, **102**, 051912.
21 Y. Sun, X. Zuo, S. K. R. S. Sankaranarayanan, S. Peng, B. Narayanan and G. Kamath, *Science*, 2017, **356**, 303–307.
22 H. T. Luu and N. Gunkelmann, *Comput. Mater. Sci.*, 2019, **162**, 295–303.
23 A. Ali, H. Zafar, M. Zia, I. U. Haq, A. R. Phull, J. S. Ali and A. Hussain, *Nanotechnol., Sci. Appl.*, 2016, **9**, 49–67.
24 H. Cao, G. Huang, S. Xuan, Q. Wu, F. Gu and C. Li, *J. Alloys Compd.*, 2008, **448**, 272–276.
25 J. Chen, P. Li and E. E. Lin, *RSC Adv.*, 2020, **10**, 40084–40091.
26 M. Kaur, J. S. McCloy, W. Jiang, Q. Yao and Y. Qiang, *J. Phys. Chem. C*, 2012, **116**, 12875–12885.
27 R. G. Mendes, B. Koch, A. Bachmatiuk, A. A. El-Gendy, Y. Krupskaya, A. Springer, R. Klingeler, O. Schmidt, B. Büchner, S. Sanchez and M. H. Rümmeli, *Biochim. Biophys. Acta*, 2014, **1840**, 160–169.
28 M. Weissmann, G. García, M. Kiwi and R. Ramirez, *Phys. Rev. B: Condens. Matter Mater. Phys.*, 2004, **70**, 201401.
29 S. Geng, W. Ding, S. Guo, X. Zou, Y. Zhang and X. Lu, *Ironmaking & Steelmaking Processes, Products and Applications*, 2015, **42**(9), 714–719.
30 A. M. Garcia, C. M. Masterson, A. Prakash, M. L. Nakamoto, D. G. Rojas, C. O. Keskinbora, D. C. Bell and V. L. Colvin, *ACS Appl. Nano Mater.*, 2019, **2**, 667–672.
31 H. Bae, T. Ahmad, I. Rhee, Y. Chang, S. U. Jin and S. Hong, *Nanoscale Res. Lett.*, 2012, 1–5.
32 H. Liu, S. H. Luo, S. X. Yan, Q. Wang, D. B. Hu, Y. L. Wang, J. Feng and T. F. Yi, *Composites, Part B*, 2019, **164**, 576–582.
33 I. H. Sahputra, A. Chakrabarty, O. Restrepo, O. Bouhali, N. Mousseau, C. S. Becquart and F. E. Mellouhi, *Phys. Status Solidi B*, 2017, **254**(2), 1–10.
34 M. Aryanpour, A. C. T. van Duin and J. D. Kubicki, *J. Phys. Chem. A*, 2010, **114**(21), 6298–6307.
35 G. Aral, M. M. Islam, Y. J. Wang, S. Ogata and A. C. T. van Duin, *J. Appl. Phys.*, 2019, **125**, 165102.
36 G. J. Martyna, M. L. Klein and M. Tuckerman, *J. Chem. Phys.*, 1992, **97**, 2635.
37 A. Stukowski, *Modell. Simul. Mater. Sci. Eng.*, 2010, **18**, 015012.
38 G. J. Martyna, D. J. Tobias and M. L. Klein, *J. Chem. Phys.*, 1994, **101**, 4177.
39 M. P. Allen and L. J. Tildesley, *Computer Simulation of Liquids*, Oxford University Press, New York, 1987.
40 S. Plimpton, *J. Comput. Phys.*, 1995, **117**, 1–19.
41 M. Tavakkoli, T. Kallio, O. Reynaud, A. G. Nasibulin, C. Johans, J. Sainio, H. Jiang, E. I. Kauppinen and K. Laasonen, *Angew. Chem.*, 2015, **127**, 4618–4621.
42 A. Furlan, U. Jansson, J. Lu, L. Hultman and M. Magnuson, *J. Phys.: Condens. Matter*, 2015, **27**, 045002.
43 G. Gunbas, N. Hafezi, W. L. Sheppard, M. M. Olmstead, I. V. Stoyanova, F. S. Tham, M. P. Meyer and M. Mascal, *Nat. Chem.*, 2013, **4**, 1018–1023.
44 J. Byggmästar, F. Granberg, A. Kuronen, K. Nordlund and K. O. E. Henriksson, *J. Appl. Phys.*, 2015, **117**, 014313.
45 K. Y. Xie, S. Shrestha, Y. Cao, P. J. Felfer, Y. Wang, X. Liao, J. M. Cairney and S. P. Ringer, *Acta Mater.*, 2013, **61**, 439–452.
46 L. Li, F. Solá, Z. H. Xia and Y. Q. Yang, *J. Appl. Phys.*, 2012, **111**, 094306.
47 W. Wei and X. Yu, *Mater. Today Commun.*, 2020, **24**, 101217.
48 Y. Rosandi, H. T. Luu, H. M. Urbassek and N. Gunkelmann, *RSC Adv.*, 2020, **10**, 14353.
49 J. Godet, C. Furgeaud, L. Pizzagalli and M. J. Demkowicz, *Ext. Mech. Lett.*, 2016, **8**, 151–159.
50 M. Hou and O. Melikhova, *Acta Mater.*, 2009, **57**, 453–465.

